Hindawi Publishing Corporation
International Journal of Photoenergy
Volume 2014, Article ID 239137, 12 pages
http://dx.doi.org/10.1155/2014/239137

Research Article

An Innovative Application of a Solar Storage Wall Combined with the Low-Temperature Organic Rankine Cycle

Tzu-Chen Hung,[1] Duen-Sheng Lee,[2] and Jaw-Ren Lin[3]

[1] *Department of Mechanical Engineering, National Taipei University of Technology, Taipei 10608, Taiwan*
[2] *Graduate Institute of Mechanical and Electrical Engineering, National Taipei University of Technology, Taipei 10608, Taiwan*
[3] *Department of Mechanical Engineering, Taoyuan Innovation Institute of Technology, Jhongli 32091, Taiwan*

Correspondence should be addressed to Tzu-Chen Hung; tchung@ntut.edu.tw

Received 9 June 2014; Accepted 25 July 2014; Published 7 September 2014

Academic Editor: Chao-Rong Chen

The objective of this study is to collect energy on the waste heat from air produced by solar ventilation systems. This heat used for electricity generation by an organic Rankine cycle (ORC) system was implemented. The advantages of this method include the use of existing building's wall, and it also provides the region of energy scarcity for reference. This is also an innovative method, and the results will contribute to the efforts made toward improving the design of solar ventilation in the field of solar thermal engineering. In addition, ORC system would help generate electricity and build a low-carbon building. This study considered several critical parameters such as length of the airflow channel, intensity of solar radiation, pattern of the absorber plate, stagnant air layer, and operating conditions. The simulation results show that the highest outlet temperature and heat collecting efficiency of solar ventilation system are about 120°C and 60%, respectively. The measured ORC efficiency of the system was 6.2%. The proposed method is feasible for the waste heat from air produced by ventilation systems.

1. Introduction

The development of the economy and society on a global scale has been accompanied by energy crises and environment pollution, which have become two major problems worldwide. Therefore, the application of renewable energies (solar energy, wind energy, and geothermal energy) in electricity generation is becoming increasingly crucial. In addition, power generation in which the organic Rankine cycle (ORC) is used to recover low-grade energy sources has attracted considerable attention. In recent years, Hung et al. [1, 2] have extensively studied the development and applications of ORC electrical generating systems.

Among these sources, geothermal and solar energy are typically used in converting low-grade heat into power and in other applications [3–8]. Wang et al. [3, 6] designed a low-temperature solar Rankine system. Both evacuated solar collectors and the flat-plate solar collectors are used in this experimental system. Hettiarachchi et al. [4] presented a cost-effective optimal design criterion for organic Rankine power cycles using low-temperature geothermal heat sources. Karellas et al. [7] reported that a heat recovery system could be used to increase the efficiency of the cement plant and, thus, contributes to the emissions reduction when using a typical cement production procedure. Wang et al. [8] investigated the performance of a low-temperature solar Rankine cycle system using working fluid R245fa. The experimental results indicated that the highest heat-collecting efficiency of a flat-plate collector is approximately 50%. Hung [9] investigated a maximum work output from various combinations of thermodynamic cycles from a viewpoint of the cycle systems. The study shows that the series-type triple cycle exhibits no significant difference as compared with the combined cycle. Hung et al. [10] analyzed parametrically and compared the efficiencies of ORCs using cryogens such as benzene, ammonia, R11, R12, R134a, and R113 as working fluids.

According to the statistical data, air conditioning takes about 40% of electricity demand for building. Therefore, natural ventilation has received considerable attention because it reduces heat gain and induces natural cooling or heating

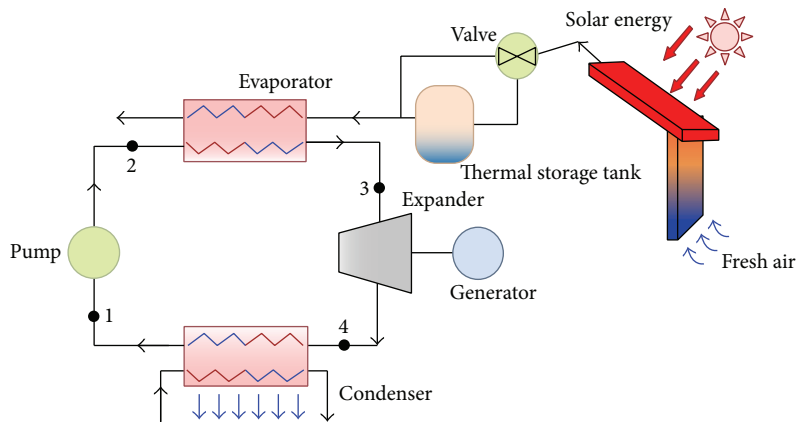

Figure 1: Schematic diagram of the ventilation in building combined with ORC system.

in both commercial and residential buildings and provides potential benefits regarding operational costs, energy requirements, and carbon dioxide emission.

The objective of this study is to collect the waste heat from air produced by ventilation systems. The waste heat was used for electricity generation in which an ORC system was implemented, as shown in Figure 1. This method also served the purpose of combining the waste heat produced by ventilation system with an ORC system to facilitate the creation of a reasonable indoor environment characterized by human thermal comfort, energy efficiency, and environmental friendliness and to construct a low-carbon building. The advantages of this method include the use of existing building's wall, and it also provides the region of energy scarcity for reference. This is an innovative method, and the results will contribute to the efforts made toward improving the design of solar ventilation in the field of solar thermal engineering. Thus far, relatively little research in this area has been conducted.

A wide variety of natural ventilation systems are presented in the literatures. Solar wind towers [11], Trombe walls [12], and solar chimneys [13] are examples. Zhai et al. [14] proposed that active solar systems can be used to enhance the ventilation performance of solar chimneys. The main configurations and integrated renewable energy systems based on solar chimneys were investigated. El-Sawi et al. [15] investigated the chevron pattern of fold structure produced using a recently developed continuous folding technique. Arce et al. [16] experimentally investigated the thermal performance of a solar chimney for natural ventilation. The experimental model was implemented under full-scale and real meteorological conditions, to compare the experimental results with simulation results. Yadav and Bhagoria [17] presented a detailed review of the literature that involves the application of CFD in the design of solar air heaters. The solar chimney concept used for improving the natural ventilation of rooms was analytically and numerically studied [18]. The present study considered several geometrical parameters such as chimney inlet size and width, which are considered to have a significant effect on space ventilation. CFD modelling techniques were used to assess the effects of inclination angle, double glazing, and low-emissivity finishes on the induced ventilation rate [19]. Hu et al. [20] investigated a simple-structure mechanical ventilation solar air collector (MV-SAC) with internal baffles. A numerical model was developed in the present study to predict solar air collector internal flow and heat transfer characteristics. Tian and Zhao [21] and Alkilani et al. [22] reported that various types of thermal energy storage systems are also reviewed and discussed, including sensible heat storage, latent heat storage, chemical storage, and cascaded storage.

In this study, we applied experiments and CFD to solve problem of solar storage wall combined with the organic Rankine cycle. The fluid flow and heat transfer of this solar storage wall were analyzed numerically, and the results were validated based on the experimental data. Subsequently the parameters, such as the thickness of the air gap, the operating conditions, and height of flow, that clearly influence collector efficiency were analyzed. These results provide a reference for the future design and optimization of solar storage wall.

2. Experimental Analysis

In this section, we present the details of the experiments and performance analysis conducted in this study.

2.1. Solar Simulator. Factors such as time, season, and weather cause the experimental results to become unstable. Therefore, we constructed a solar simulator that can provide stable energy on an absorber plate, as shown in Figure 2(a). The spectral range of the solar simulator was visible light, the wavelength of which 500–600 nm, and the distributed heat flux was between 780 and 820 W/m^2, as shown in Figure 2(c). The measured results indicate that the variation in the maximal heat flux at various locations was less than 50 W/m^2 and that the solar simulator produced uniform heat flux.

2.2. Experimental Setup. The collector module consisted of glass, an absorber plate, an airflow channel, a stagnant air layer, insulation, and an aluminum collector frame used to

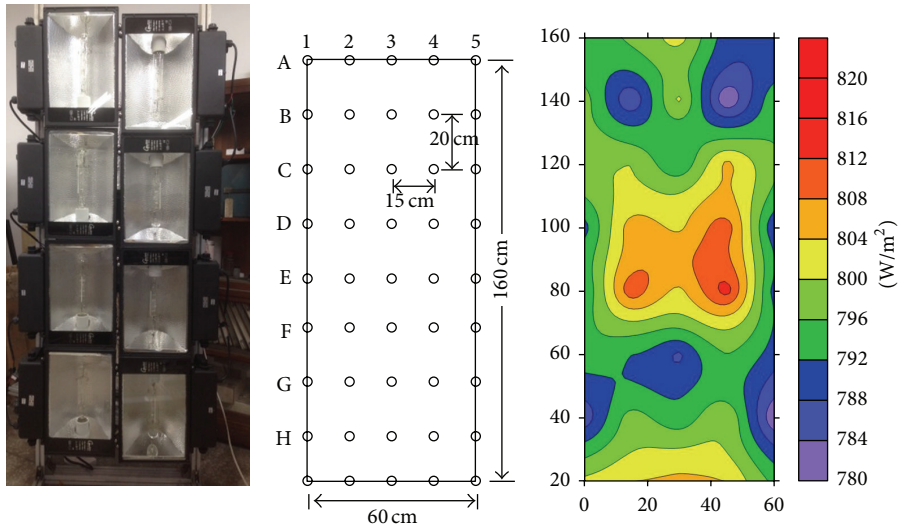

(a) Solar simulator (b) Measurement location (c) Heat flux (W/m^2)

Figure 2: Distribution of heat flux on glazing for solar simulator.

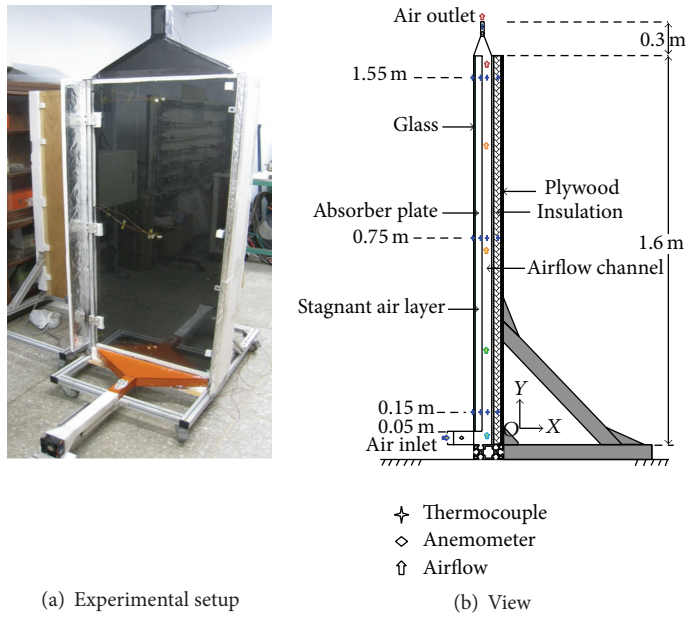

(a) Experimental setup (b) View

Figure 3: Schematic diagram of the experimental setup and view of the solar chimney.

install the components, as shown in Figure 3(a). The absorber plate was 1.6 m high, 0.6 m wide, and 0.08 m thick; the stagnant air layer was 0.18 m deep; and the glass cover was 0.004 m thick. To collect sufficient solar radiation, the surface of the absorber plate was painted black. The purpose of using a glass cover and a stagnant air layer was to decrease convection heat losses from the absorber plate. The surface of the aluminum collector frame was insulated to achieve minimal heat loss. The insulation was protected using a fiberglass wool envelope.

The air inlet to the chimney was located at the bottom of solar storage wall and the air outlet was located at the top. Inlet airflow was collimated by employing a laminated array to provide the velocity component in the x-direction only. The inlet and outlet cross-section were maintained equal and constant ($A_{in} = A_{out} = 0.002\,m^2$) to reduce the pressure loss in the inlet and outlet areas. Before conducting the performance tests, both the thermocouples and flow meters used were calibrated to ensure accurate measurements. The collectors, based on their respective settings, were tested for leaks under the operating pressure.

2.3. Instrumentation. The variables measured in this experiment included the inlet and outlet air temperature, ambient

temperature, and the solar radiation and mass flow rate of the air. The collector was instrumented with three T-type thermocouples (H = 0.15, 0.75, and 1.55 m) for measuring the temperatures in each component. The airflow rate was calculated using the measured air velocity and the known duct area. The data acquisition system consisted of a data logger, which was connected to a personal computer through an RS232 serial port. The locations of each sensor are shown in Figure 3(b).

2.4. Performance Analysis. The useful energy gained using the solar ventilation system can be expressed as [23]

$$Q_u = \dot{m} C_p \left(T_{\text{out}} - T_{\text{in}}\right), \tag{1}$$

and the following heat balance equation expresses the thermal performance of a collector under steady-state conditions:

$$Q_u = AF_R \left[I(\tau\alpha)_c - U_L \left(T_i - T_{\text{amb.}}\right)\right], \tag{2}$$

where F_R is the collector heat removal factor and U_L is the top loss coefficient, which is dependent on temperature and wind speed. A measure of collector performance is collector efficiency, defined as the ratio of useful heat gain over any time period to the incident solar radiation over the same period. Thus, the efficiency equation is written as follows:

$$\eta_c = \frac{Q_u}{IA}. \tag{3}$$

From (1) and (3), the collector efficiency can be expressed as follows:

$$\eta_c = \dot{m} C_p \frac{\left(T_{\text{out}} - T_{\text{in}}\right)}{IA}. \tag{4}$$

The general test procedure involves determining Q_u using (1) and measuring I, T_i, and $T_{\text{amb.}}$ by operating the collector under nearly steady-state conditions in test facilities.

3. Numerical Analysis

In this study, commercial CFD code ANSYS FLUENT [24] software was used as to perform the numerical calculations. CFD is a simulation tool that uses powerful computer and applied mathematics to model fluid-flow situations to predict heat.

3.1. Governing Equation. In the ventilation system, the study used rectangle pipe flow, and the hydraulic diameter, $D_h = 4A/P$, was calculated by four times the ratio of the cross-section flow area divided by the wetted perimeter, P, of the pipe. The Reynolds number, $\text{Re} = \rho v D_h/\mu$, was greater than 2300. Therefore, the standard k-ε equation was adopted in the chimney region. The flow phenomenon that occurs in a ventilation channel is governed by the continuity, momentum, and energy equations involved in the steady-state regime which can be written as follows [17].

Continuity equation:

$$\frac{\partial}{\partial x_i}\left(\rho u_i\right) = 0. \tag{5}$$

Momentum equation:

$$\frac{\partial}{\partial x_i}\left(\rho u_i u_j\right) = -\frac{\partial P}{\partial x_i} + \frac{\partial}{\partial x_j}\left[\mu\left(\frac{\partial u_i}{\partial x_j} + \frac{\partial u_j}{\partial x_i}\right)\right] + \frac{\partial}{\partial x_j}\left(-\rho\overline{u_i' u_j'}\right). \tag{6}$$

Energy equation:

$$\frac{\partial}{\partial x_i}\left(\rho u_i T\right) = \frac{\partial}{\partial x_j}\left[\left(\Gamma + \Gamma_t\right)\frac{\partial T}{\partial x_j}\right], \tag{7}$$

$$\Gamma = \frac{\mu}{\text{Pr}}, \qquad \Gamma_t = \frac{\mu_t}{\text{Pr}_t}, \tag{8}$$

where Γ, Γ_t, and Pr are the molecular thermal diffusivity, turbulent thermal diffusivity, and Prandtl number, respectively. μ_t in (8) is the turbulent viscosity.

The discrete ordinates (DO) model was chosen for conducting the simulation of radiation heat transfer. This was achieved by coupling radiative transfer equation (RTE) and the convective energy equation [25]. Solar ray tracing was used to calculate radiation effects produced by the sun's rays that irradiate the computational domain. The solar load model's ray tracing algorithm was used to predict the direct illumination energy source that results from incident solar radiation.

3.2. Geometric Modeling and Meshing. The complete geometry of the system is divided into three sections: the entrance, test, and exit sections. The 3D domain used for CFD analysis was set up to have a height of 1.9 m, width of 0.6 m, and a depth of 0.04 m. The depth of the stagnant air layer and airflow is 0.18 m and 0.02 m, respectively. To reduce the burden of computational time and memory space on the computer, the system under consideration was assumed to have a symmetric plane.

The 3D computational domain of the solar ventilation system was created and meshed according to its actual size by using Gambit [26] software. A uniform mesh comprising extremely fine mesh near the wall was used to resolve the laminar sublayer as shown in Figure 4. The nearest grid point to the wall was carefully adjusted to place it in the linear region and thereby ensure that the nondimensional wall distance y^+ was less than 3.0. The total grid number was determined to be 1,525,068 cells after the grid independence was investigated.

3.3. Boundary Conditions and Material Properties. Uniform air velocity was introduced at the inlet while a constant pressure was applied at the outlet. The system under consideration was assumed to have a symmetric plane. In addition, the collector frame was assumed to be adiabatic. The heat loss from the back plate and the glass to the surroundings was considered, and no-slip boundary condition was assigned to the walls in contact with the fluid in the model.

The properties of the working fluid (air), absorber plate (aluminum), and glass material were assumed to remain constant. The glass and absorber plate were homogeneous and

Table 1: Thermophysical properties of working fluid (air) and absorber plate (aluminum) for computational analysis.

Properties	Working fluid (air)	Absorber plate (aluminum)	Glass
Density, ρ(kg/m^3)	Incompressible ideal glass	2719	2500
Specific heat, C_p (J/kg-K)	1006.43	871	750
Viscosity, μ (N/m^2)	1.7894×10^{-5}	—	—
Thermal conductivity, k (W/m-K)	0.0242	202.4	1.4
Absorptivity, α	—	0.9	0.12
Emissivity, ε	—	0.4	0.9

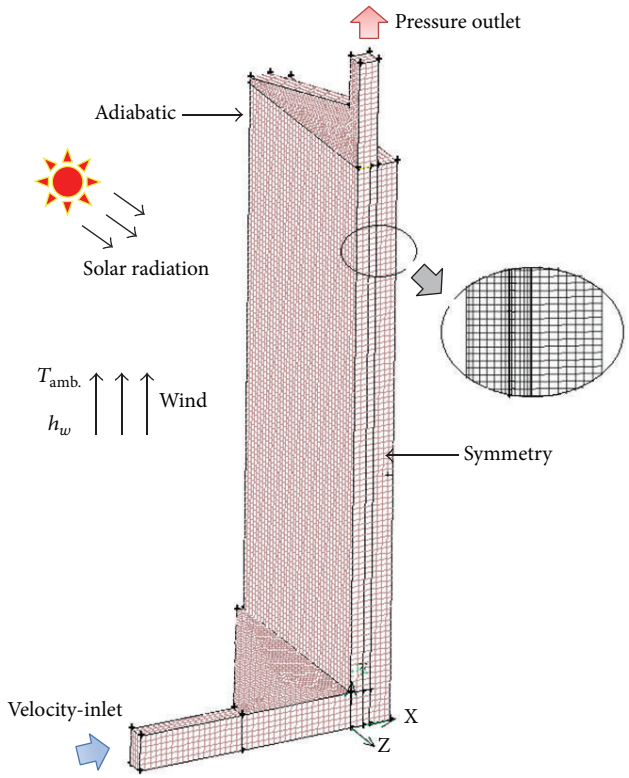

Figure 4: Computational model and boundary conditions.

isotropic. The thermal conductivity of the frame, absorber plate, and glass was temperature independent. The thermophysical properties of the working fluid, glass, and absorber plate are listed in Table 1. Because the flow velocity in the ventilation system and the decrease in pressure were relatively small, the air was considered as incompressible fluid, and the density was assumed to be approximately that of ideal gas, considering the thermal expansion effect.

After establishing all the relevant settings, ANSYS FLUENT performed the calculation in an iterative manner until a sufficient tolerance, defined by the user, was achieved. The convergence criterion of 10^{-6} represents the residuals in the continuity equation; 10^{-3} for the residuals of the velocity components and 10^{-6} for the residuals of the energy were assumed.

3.4. Validation of the Computation Fluid Dynamics Results. We investigated the feasibility of solar ventilation in natural convection and compared the measured and calculated results. The results of solar simulator show that the uniform heat flux can be assumed as 800 W/m^2. The heat transfer coefficient of the wind and temperature of ambience were assumed to be 20 W/m^2-K and 30°C, respectively. The error of the temperature between the CFD and experimental results is given by

$$\zeta = \frac{\left|T_{\text{CFD}} - T_{\text{Exp.}}\right|}{T_{\text{Exp.}} - T_{\text{amb.}}} \times 100\%. \quad (9)$$

Figure 5 shows the air temperature comparison between measured and calculated results under free convection. It shows that the deviation of the solutions obtained using CFD simulations was generally within the acceptable range, in which the inlet air velocity is 0.45 m/s. This proves that CFD is an effective tool for predicting the behavior and performance of a ventilation system. The flow field and temperature distribution in the computational domain are shown in Figure 6. The computed temperature variation behavior was clearly within reasonable accuracy. The simulation results also indicated that the temperature of the air increased as the airflow height increased.

In this study, the maximal temperature and mass flow rate were determined using various lengths of airflow under ideal conditions for the proposed system. Figure 7 shows the temperature and mass flow rate for various lengths of airflow under ideal conditions. It is clearly seen that the disparity of temperature between the ideal (Figure 5) and actual measurements (Figure 7) was approximately 40°C. The main reason is that actual measurements have energy loss. The analysis results for the parameters that clearly influence collector efficiency, such as the thickness of the air gap, the operating conditions, and height of flow, are presented and considered to be references for the future design and optimization of solar ventilation systems which are provided in the following section.

4. Results and Discussion

The accuracy of the calculated numerical results was accepted. Therefore, the experiment and simulation were applied to obtain optimal geometric design. CFD provides numerical advantages over experiment-based approaches,

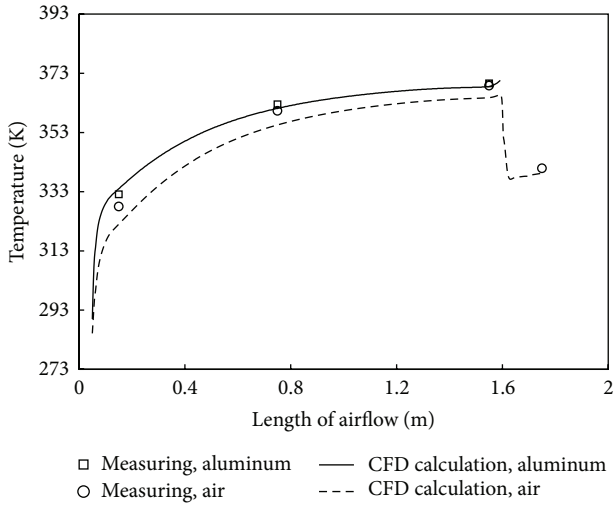

Figure 5: Air temperature comparison between measured and calculated results under free convection.

such as the substantial reduction in human labor and work time and the costs of materials. This study investigated the influence of various lengths of airflow, operating conditions of the inlet, the energy of heat flux, the type of absorber used for achieving efficiency, and the width of the air layer.

4.1. Natural Convection and Forced Convection. According to the results described in Section 3.4, the performance of waste heat recovery was not significant because of the low mass flow rate of the system. Therefore, the potential enhancement of mass flow rate was investigated by changing the velocity of the air inlet. A fan was installed at the air inlet to facilitate heat circulation. The following velocities at the air inlet were used, that is, 1, 1.5, 2, 3, 4, 5, and 6 m/s. Figure 8 shows the effect of the mass flow rate on the outlet temperature and on the efficiency of the ventilation system, which were measured experimentally. The outlet temperature clearly decreased as the mass flow rate increased, and the efficiency increased at a decreasing rate. The results clearly indicate that forced convection is more efficient than natural convection.

The measurement results and CFD simulation, in which forced convection (V_{in} = 2 m/s) was used, are shown in Figure 9. The results obtained using the CFD approach were similar to the experimental results, indicating that CFD can be used for predicting the behavior and performance of a ventilation system in which forced convection is involved. The results indicate that exit temperature decreased because the temperature of the airflow channel was not uniform at the same elevation, as shown in Figure 10.

The longer the residence time in the airflow channel, the smaller the temperature difference between the aluminum and the air. Thus, the heat transferred to the air via the aluminum is reduced. If the air does not very smoothly flow in and out through the flow channel, it may cause a high percentage of heat returned to the environment by way of thermal radiation.

4.2. Actual Test of Natural Convection. The experimental study was conducted on the Penghu Islands. The Penghu Island of Taiwan was located at 23°28′17″ latitude north and 119°30′45″ longitude west. Figure 11 shows a photo of the solar ventilation system. The angle and length of airflow were 15° and 4 m for solar ventilation system, respectively. The time step for data collection was set as 1 min. The maximal glass, absorber plate, airflow channel, and plywood temperature were obtained at a height of 1.55 m, as shown in Figure 3(b). Figure 12(a) shows that the maximal temperature values were obtained approximately at noon. It is obvious that the overall changing trend with time of the temperature follows that of the solar radiation. At about 11:15, the solar radiation was blanked. However, the temperature will not be affected immediately, because the system still provides energy. The results also indicated that the air temperature difference between the exit and the inlet was approximately 50°C. The velocity of the ambience and the air of airflow channel is shown in Figure 12(b). The velocity of ambience was greater than that of airflow channel.

4.3. Length of the Airflow Channel. Regarding heat transfer, a large absorber area may result in a substantial increase in temperature during solar ventilation. Therefore, potential enhancement of heat removal was investigated by the changing length of airflow and solar radiation, and v_{in} was assumed to be 2 m/s. Five airflow channel lengths were used for heat transfer analysis: 0.8, 1.6, 2.4, 3.2, and 4.0 m. Figure 13(a) shows the effect of the airflow length and solar radiation on the outlet temperature by CFD simulation. Clearly, the outlet temperature increased when the airflow length increased. However, the change was not obvious when the height exceeded approximately 3.5 m. Therefore, an optimal length of approximately 3.5–4 m can be selected.

Furthermore, the intensity of solar radiation depends on the orientation of the solar ventilation system, the day of the year, and the hour of the day, among other working conditions. Therefore, this study investigated the effect of solar radiation, and the results are shown in Figure 13(a). The outlet temperature was increased by approximately 4% when the solar radiation increased as 200 W/m^2. Figure 13(b) shows the effect of the airflow length and solar radiation on the efficiency by CFD simulation. It shows that the efficiency in energy collection decreased when the airflow length increased.

4.4. Pattern of the Absorber Plate. The convective heat transfer rate in the airflow channel can be augmented by increasing the heat transfer surface area and increasing the turbulence inside the channel. This study investigated the effect of various types of absorber plates which are inexpensive and common. Figure 14 shows that three independent sets of experiments were conducted to investigate the performance of both the flat and rectangular tubes; the cross-section was 6 × 2 and 10 × 1 cm, respectively.

Figure 15(a) shows the difference between inlet air temperature of the solar ventilation and outlet air temperature of the solar ventilation for various patterns of the absorber plate.

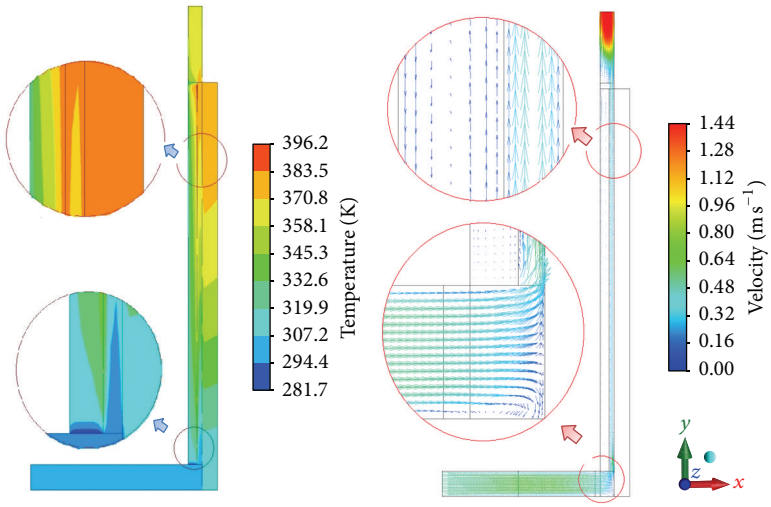

FIGURE 6: The flow field and temperature distribution in the computational domain.

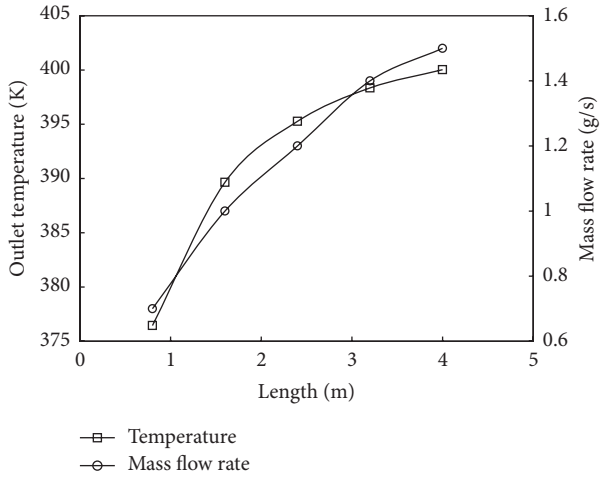

FIGURE 7: The maximum temperature and mass flow rate with various lengths of airflow.

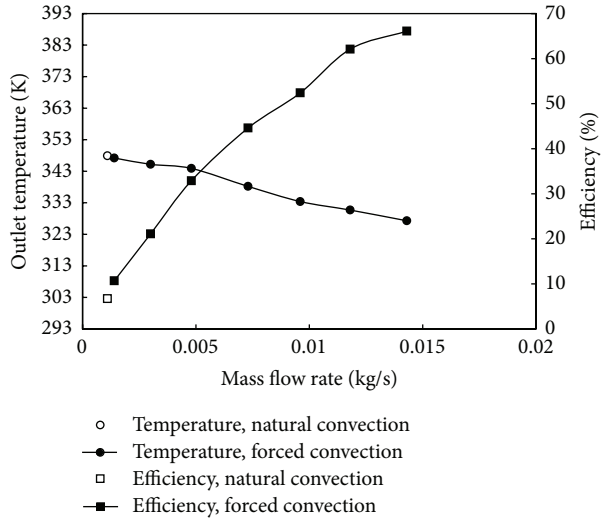

FIGURE 8: Outlet temperature and efficiency of the collector versus mass flow rate at $T_i = T_{\text{amb.}} = 20^{\circ}\text{C}$.

It shows that the temperature produced in Case I was clearly higher than that in Cases II and III. The main reason for this result is that the heat transfer surface area was increased, for the temperature difference of Case III exceeds Case II when the mass flow rate is higher than about 0.008 kg/s. The main reason is that the material is different between Cases II and III. The effect of material is more significant than that of heat transfer surface. The efficiency for three types of collectors is shown in Figure 15(b). The efficiency of three various absorber plates increased when the mass flow rate increased. It also shows that Case I absorber plate was more efficient than those used in Cases II and III. The optimal design and control range of the solar thermal collector were approximately 2-3 m/s for effective ORC waste heat recovery.

4.5. Stagnant Air Layer and Operating Conditions. Heat loss occurs in the air space between the glazing and absorber plate through convection and conduction back the atmosphere. To reduce the heat loss of the absorber plate, the influence of various widths of the stagnant air layer and the associated heat transfer coefficient of wind on thermal performance was investigated. Five air layer widths were used in the CFD simulation: 0.3, 0.8, 1.8, 2.8, and 3.8 cm. The heat transfer coefficients were 10, 20, and 30 W/m^2-K, respectively.

The various air layer widths and wind velocity are shown in Figure 16. The change in loss heat was not obvious when the heat transfer coefficient of wind was lower than approximately 20 W/m^2-K. In addition, the heat loss of the absorber plate was not obvious when the air layer width was higher than that of 2 m. The main reason for these results is that the effective buoyancy force driven by the air density difference between the glass and absorber plate airflow channel was disrupted when the width of the air layer was too thin.

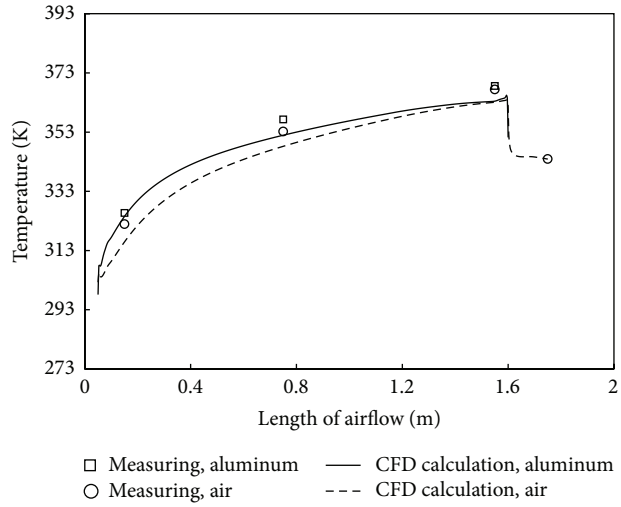

Figure 9: Temperature comparison between measurement and CFD calculation at $v_{in} = 2$ m/s.

The overall effects of the width and heat transfer coefficient of wind on the outlet temperature were not obvious and exhibited 3% variation.

4.6. Economic Assessment of ORC Combined with the Solar Storage Wall. In this section, we investigated the economic assessment for solar storage wall combined with the organic Rankine cycle, as shown in Figure 1. Figure 17 illustrates the thermodynamic process described above. A theoretical Rankine cycle consists of the following processes:

$1 \rightarrow 2$: compression (working fluid feed pump);

$2 \rightarrow 3$: heat supply (solar ventilation system);

$3 \rightarrow 4$: expansion (expander);

$4 \rightarrow 5$: heat rejection (condenser).

At the same time, the process $3 \rightarrow 4a$ which appeared in Figure 17 is the ideal isentropic expansion process. Although this process cannot be reached during real operation, it is an evaluation criterion of the real expansion process. For the Rankine cycle system utilizing R245fa, the efficiency of the ORC is written as follows:

$$\eta_R = \frac{w_{34} + w_{12}}{q_{23}}, \tag{10}$$

where w_{34} is the power output obtained from the expander, w_{12} is power consumed by the feed pump, and q_{23} is the heat quantity absorbed by R245fa from solar collector. The power generation efficiency of the system is written as follows:

$$\eta_{sys} = \eta_c \times \eta_R. \tag{11}$$

From above, result indicates that the highest outlet temperature and efficiency of air collected were approximately 100°C and 60% (with 4 m length of air channel and absorber plate of Case I). In this study, heat exchanger's performance was assumed as 80%, and the temperature of hot water was approximately 80°C. Figure 17 shows the schematic *T*-*S* diagram of the low-temperature Rankine cycle system, and the efficiency of ORC was 6.2%. The assessment for ORC combined with the solar storage wall is shown in Table 2. For this study, the area of collector for building was assumed to have a width of 6 m and height of 8 m. The result indicates that the effective system efficiency for thermal to power is about 3.7% with the power generation of about 11.43 kWh per day. If the future wall structure can be modified with appropriate design, its cost is expected to be lower than current type. The proposed method is feasible for the solar heat collected by air ventilation systems, and the heat was used for electricity generation in a system incorporated with ORC.

Table 2: Energy and outputs of the experimental cycle.

Properties	Working fluid (air)
Area of collector, m^2	48 (8 m × 6 m)
Solar radiation, kW/m^2	0.80
Efficiency of collector, η_c	60%
Energy, kWh/day (8 hours/day)	184.3
Efficiency of Rankine cycle, η_R	6.2%
Power generated, kWh/day	11.43

5. Conclusions

An innovative application of ORC systems combined with solar ventilation was investigated and an experimental prototype was designed, constructed, and tested in this study. Experiments and CFD simulations were used to investigate the performance of the proposed solar ventilation system. The results are summarized as follows.

(1) The deviation of the solutions obtained using CFD simulations was generally within the acceptable range, which proves that CFD is a qualified tool for predicting the behavior and performance of a ventilation system.

(2) The thermal performance and outlet temperature of air, when a slight forced convection was supplemented, were superior to those produced when a pure natural convection was considered.

(3) An optimal configuration of a solar ventilation system has a stagnant air layer of 2 cm, an air channel length of 4 m, and an absorber plate of Case I, and the optimal range of air inlet for thermal performance of a collector is approximately 2-3 m/s.

(4) The proposed method is feasible for the solar heat collected by air ventilation systems, and the heat was used for electricity generation in a system incorporated with ORC.

Highlights

(i) Numerical and experimental methodologies are treated.

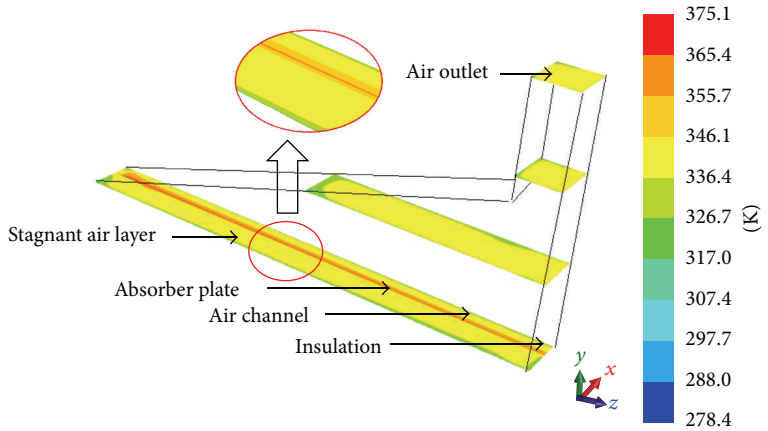

Figure 10: The temperature distribution in the exit section of solar ventilation.

Figure 11: Photo of the solar chimney.

(ii) An innovative concept of combining the waste heat of ventilation with ORC system is introduced.

(iii) Various types of solar ventilation system are discussed.

Nomenclature

A: Area (m^2)
C_p: Specific heat (J/kg-K)
D_h: Hydraulic diameter of duct (m)
F_R: Collector heat removal factor
H: Height of absorber plate (m)
h: Enthalpy (kJ/kg-K), heat transfer coefficient (W/m^2-K)
I: Intensity of solar radiation (W/m^2)
k: Thermal conductivity (W/m^2-K)
Pr: Prandtl number
$\dot{m}$: Mass flow rate (kg/s)
P: Wetted perimeter
Q_u: Useful energy gain (W)
T: Temperature (K)
U_L: Top loss coefficient
v: Velocity (m/s)
w: Power (kW).

Greek Symbols

α: Absorptivity
$(\tau\alpha)_e$: Effective transmittance-absorptance product
ρ: Density of material
ε: Emissivity
μ: Viscosity
μ_t: Turbulent viscosity
Γ: Molecular thermal diffusivity
Γ_t: Turbulent thermal diffusivity
η: Thermal efficiency
η_c: Collection efficiency of the solar collector
η_R: Rankine cycle efficiency
η_s: Overall efficiency of the system
Δ: Different
ξ: Error of temperature.

Subscript

amb.: Ambient
c: Solar ventilation
in: Inlet
out: Outlet
R: Rankine cycle
w: Wind
t: Turbulent.

Conflict of Interests

The authors declare that there is no conflict of interests regarding the publication of this paper.

Acknowledgment

This research work has been supported by the National Science Council, Taiwan, under Grant of Contract nos. NSC 103-3113-P-007-002 and NSC 101-2221-E-027-039.

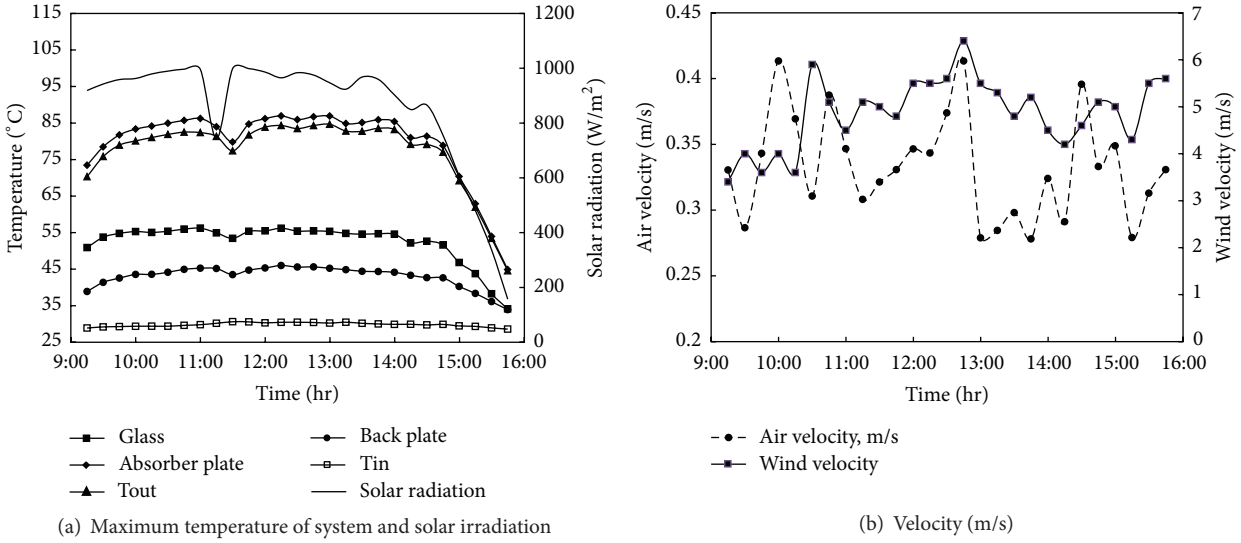

(a) Maximum temperature of system and solar irradiation

(b) Velocity (m/s)

Figure 12: Surface temperature variation at different location and weather condition (September 18, 2013).

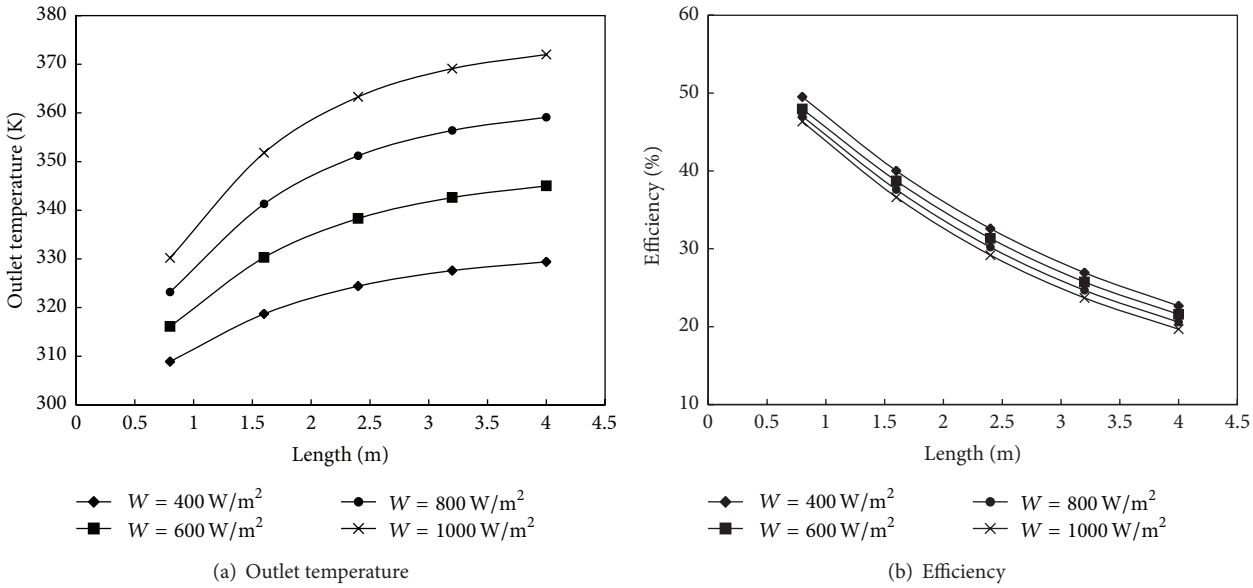

(a) Outlet temperature

(b) Efficiency

Figure 13: Effect of the lengths of airflow channel and solar heat flux by CFD simulation at $\dot{m} = 0.003$ kg/s, $T_{amb.} = 293$ K.

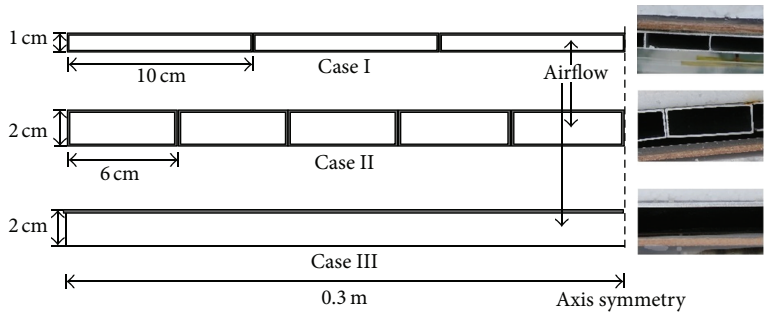

Figure 14: Three types of absorber plate in the solar ventilation.

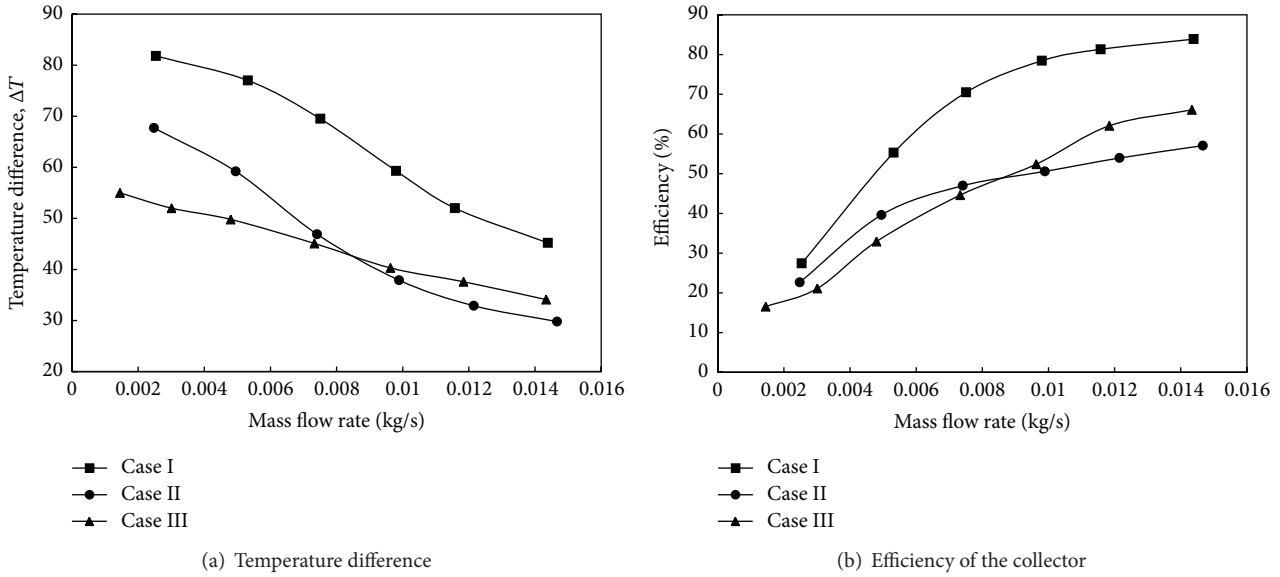

(a) Temperature difference (b) Efficiency of the collector

Figure 15: Temperature difference and efficiency of the collector versus mass flow rate for various absorber plates by experiment measurement.

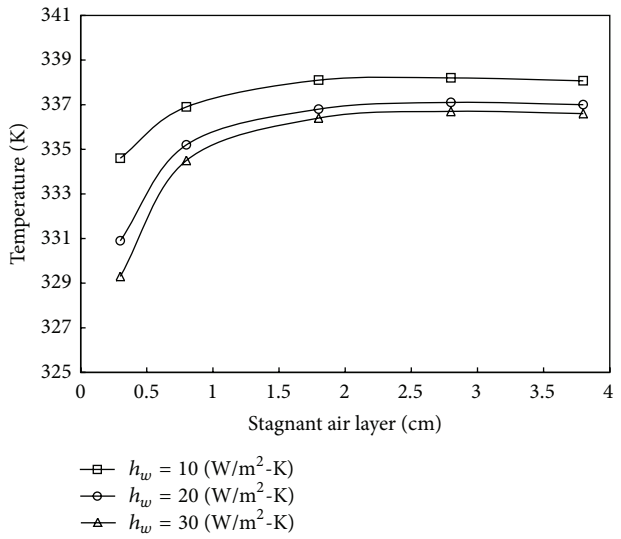

Figure 16: The outlet temperature for various widths of air layer and heat transfer coefficient of wind by CFD simulation.

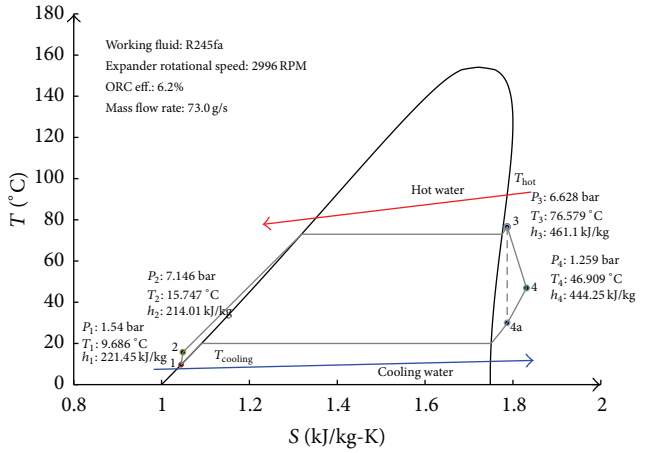

Figure 17: Schematic T-S diagram of the low-temperature Rankine cycle system.

References

[1] T.-C. Hung, "Waste heat recovery of organic Rankine cycle using dry fluids," *Energy Conversion and Management*, vol. 42, no. 5, pp. 539–553, 2001.

[2] T. C. Hung, S. K. Wang, C. H. Kuo, B. S. Pei, and K. F. Tsai, "A study of organic working fluids on system efficiency of an ORC using low-grade energy sources," *Energy*, vol. 35, no. 3, pp. 1403–1411, 2010.

[3] X. D. Wang, L. Zhao, J. L. Wang, W. Z. Zhang, X. Z. Zhao, and W. Wu, "Performance evaluation of a low-temperature solar Rankine cycle system utilizing R245fa," *Solar Energy*, vol. 84, no. 3, pp. 353–364, 2010.

[4] H. D. M. Hettiarachchi, M. Golubovic, W. M. Worek, and Y. Ikegami, "Optimum design criteria for an organic rankine cycle using low-temperature geothermal heat sources," *Energy*, vol. 32, no. 9, pp. 1698–1706, 2007.

[5] T. Guo, H. X. Wang, and S. J. Zhang, "Fluids and parameters optimization for a novel cogeneration system driven by low-temperature geothermal sources," *Energy*, vol. 36, no. 5, pp. 2639–2649, 2011.

[6] M. Wang, J. Wang, Y. Zhao, P. Zhao, and Y. Dai, "Thermodynamic analysis and optimization of a solar-driven regenerative organic Rankine cycle (ORC) based on flat-plate solar collectors," *Applied Thermal Engineering*, vol. 50, no. 1, pp. 816–825, 2013.

[7] S. Karellas, A.-D. Leontaritis, G. Panousis, E. Bellos, and E. Kakaras, "Energetic and exergetic analysis of waste heat recovery systems in the cement industry," *Energy*, vol. 58, pp. 147–156, 2013.

[8] X. D. Wang, L. Zhao, and J. L. Wang, "Experimental investigation on the low-temperature solar Rankine cycle system using R245fa," *Energy Conversion and Management*, vol. 52, no. 2, pp. 946–952, 2011.

[9] T. C. Hung, "Triple cycle: a conceptual arrangement of multiple cycle toward optimal energy conversion," *Journal of Engineering for Gas Turbines and Power*, vol. 124, no. 2, pp. 429–436, 2002.

[10] T. C. Hung, T. Y. Shai, and S. K. Wang, "A review of organic rankine cycles (ORCs) for the recovery of low-grade waste heat," *Energy*, vol. 22, no. 7, pp. 661–667, 1997.

[11] B. R. Hughes, J. K. Calautit, and S. A. Ghani, "The development of commercial wind towers for natural ventilation: a review," *Applied Energy*, vol. 92, pp. 606–627, 2012.

[12] O. Saadatian, K. Sopian, C. H. Lim, N. Asim, and M. Y. Sulaiman, "Trombe walls: a review of opportunities and challenges in research and development," *Renewable and Sustainable Energy Reviews*, vol. 16, no. 8, pp. 6340–6351, 2012.

[13] R. Khanal and C. Lei, "Solar chimney: a passive strategy for natural ventilation," *Energy and Buildings*, vol. 43, no. 8, pp. 1811–1819, 2011.

[14] X. Q. Zhai, Z. P. Song, and R. Z. Wang, "A review for the applications of solar chimneys in buildings," *Renewable & Sustainable Energy Reviews*, vol. 15, no. 8, pp. 3757–3767, 2011.

[15] A. M. El-Sawi, A. S. Wifi, M. Y. Younan, E. A. Elsayed, and B. B. Basily, "Application of folded sheet metal in flat bed solar air collectors," *Applied Thermal Engineering*, vol. 30, no. 8-9, pp. 864–871, 2010.

[16] J. Arce, M. J. Jiménez, J. D. Guzmán, M. R. Heras, G. Alvarez, and J. Xamán, "Experimental study for natural ventilation on a solar chimney," *Renewable Energy*, vol. 34, no. 12, pp. 2928–2934, 2009.

[17] A. S. Yadav and J. L. Bhagoria, "Heat transfer and fluid flow analysis of solar air heater: a review of CFD approach," *Renewable and Sustainable Energy Reviews*, vol. 23, pp. 60–79, 2013.

[18] R. Bassiouny and N. S. A. Koura, "An analytical and numerical study of solar chimney use for room natural ventilation," *Energy and Buildings*, vol. 40, no. 5, pp. 865–873, 2008.

[19] D. J. Harris and N. Helwig, "Solar chimney and building ventilation," *Applied Energy*, vol. 84, no. 2, pp. 135–146, 2007.

[20] J. J. Hu, X. S. Sun, J. L. Xu, and Z. X. Li, "Numerical analysis of mechanical ventilation solar air collector with internal baffles," *Energy and Buildings*, vol. 62, pp. 230–238, 2013.

[21] Y. Tian and C. Y. Zhao, "A review of solar collectors and thermal energy storage in solar thermal applications," *Applied Energy*, vol. 104, pp. 538–553, 2013.

[22] M. M. Alkilani, K. Sopian, M. A. Alghoul, M. Sohif, and M. H. Ruslan, "Review of solar air collectors with thermal storage units," *Renewable and Sustainable Energy Reviews*, vol. 15, no. 3, pp. 1476–1490, 2011.

[23] J. A. Duffie and W. A. Beckman, *Solar Engineering of Thermal Processes*, John Wiley & Sons, New York, NY, USA, 4th edition, 2013.

[24] ANSYS Inc, *FLUENT V12 User's Guide*, 2009.

[25] D.-S. Lee, M.-L. Liu, T.-C. Hung, C.-H. Tsai, and Y.-T. Chen, "Optimal structural analysis with associated passive heat removal for AP1000 shield building," *Applied Thermal Engineering*, vol. 50, no. 1, pp. 207–216, 2013.

[26] *GAMBIT Users Guide Version 2.4.*, FLUENT Incorporated, Lebanon, NH, USA, 2006.